ELSEVIER

Nuclear Instruments and Methods in Physics Research A 470 (2001) 488–499

NUCLEAR INSTRUMENTS & METHODS IN PHYSICS RESEARCH Section A

www.elsevier.com/locate/nima

The RHIC zero degree calorimeters

C. Adler[a], A. Denisov[b], E. Garcia[c], M. Murray[d], H. Stroebele[a], S. White[e,*]

[e] *Brookhaven National Lab, Upton, NY 11973, USA*
[b] *IHEP-Protvino, Russia*
[a] *IKF, University of Frankfurt, Germany*
[d] *Texas A&M Cyclotron, College Station, TX 77843, USA*
[c] *University of Maryland, College Park, MD, USA*

Received 8 August 2000; received in revised form 18 December 2000; accepted 18 December 2000

Abstract

The RHIC zero degree calorimeters provide common event characterization in the four heavy ion experiments which recently completed their first data taking run. Here we describe simulations which lead to the design of these devices, testbeam performance and initial experience at RHIC. © 2001 Elsevier Science B.V. All rights reserved.

PACS: 25.75.−q; 29.40.Vj; 29.27.−a

Keywords: Heavy ions; Calorimeter; Luminosity

1. Introduction

High energy collisions of nuclei usually lead to the emission of evaporation neutrons from both "beam" and "target" nuclei. At the RHIC heavy ion collider with 100 GeV/nucleon beam energy, evaporation neutrons diverge by less than 2 mrad from the beam axis. Neutral beam fragments can be detected downstream of RHIC ion collisions (and a large aperture accelerator dipole magnet) if $\theta \leqslant 4$ mrad but charged fragments in the same angular range are usually too close to the beam trajectory. In this 'zero degree' region, produced particles and other secondaries deposit negligible energy when compared with that of beam fragmentation neutrons.

The purpose of the RHIC zero degree calorimeters (ZDCs) is to detect neutrons emitted within this cone along both beam directions and measure their total energy (from which we calculate multiplicity). The ZDC coincidence of the two beam directions is a minimal bias selection of heavy ion collisions. This makes it useful as an event trigger and a luminosity monitor [1] and for this reason we built identical detectors for all four RHIC experiments. The neutron multiplicity is also known to be correlated with event geometry [2,9] and will be used to measure collision centrality in mutual beam interactions.

2. Design goals

The RHIC ZDCs are hadron calorimeters. Their longitudinal segmentation ($2\lambda_I$, $50X_0$) is

*Corresponding author. Tel.: +1-516-344-5488; fax: +1-516-344-3253.

E-mail address: white1@bnl.gov (S. White).

PII: S0168-9002(01)00627-1

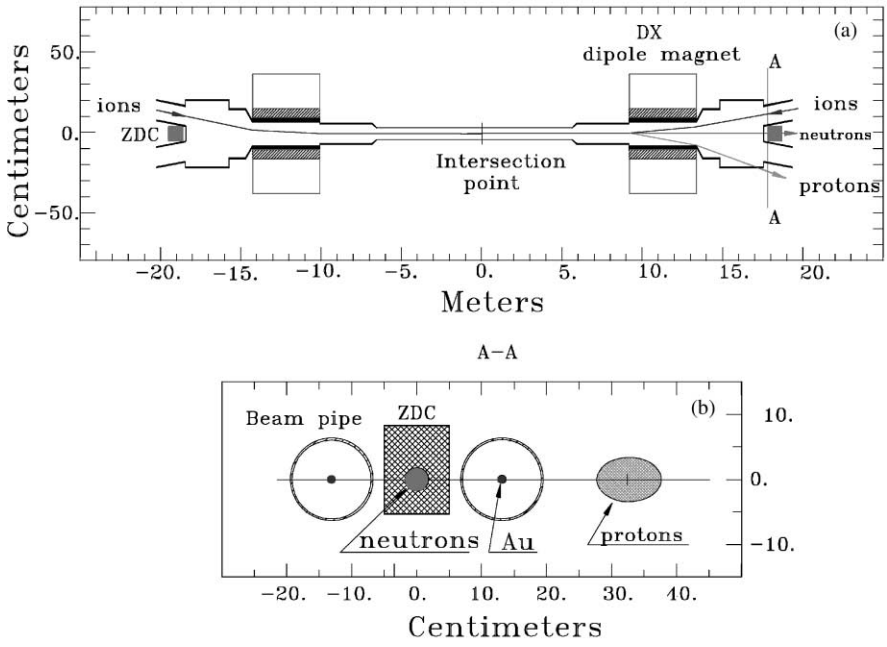

Fig. 1. Plan view of the collision region and (section A-A) "beam's eye" view of the ZDC location indicating deflection of protons and charged fragments with $Z/A \sim 1$ downstream of the "DX" Dipole magnet.

determined by practical, mechanical considerations. Electromagnetic energy emission into this region is predicted to be negligible so this measurement is not emphasized in our design. Since the spatial distribution of neutrons emitted in the fragmentation region carries only limited information about the collision, the calorimeters are built without transverse segmentation.

The forward energy resolution goal was determined by the need to clearly resolve the single neutron peak in peripheral nuclear collisions. The natural energy spread of emitted single neutrons [1] being approximately a 10% resolution of $\sigma_E/E \leqslant 20\%$ at $E_n = 100$ GeV appeared reasonable.

The limited available space between the RHIC beams at the ZDC location imposes the most stringent constraint on the calorimeter design. As can be seen from Fig. 1, the total width of the calorimeters cannot exceed 10 cm (equal to 1 nuclear interaction length (Λ_I) in tungsten). We designed the ZDCs to minimize the loss in energy resolution due to shower leakage, which can cause fluctuation in the measured shower energy through dependence on position of impact and random fluctuations in shower development.

Finally, the ZDCs are required to withstand a dose of $\sim 10^5$ rad, which is the expected exposure during several years of RHIC operation [3].

3. Simulations

We simulated shower development, light production and transport in the optical components using Geant 3.21 [4] for two basic sampling calorimeter designs:

(1) Pb absorber with scintillator sampling, and
(2) Pb, Cu or W absorber, each with undoped fiber optical ribbons in the sampling layer.

The ZDC sampling technique which we adopted for this project, is sensitive to Cherenkov light produced by charged shower secondaries in a

Table 1
Mechanical parameters of the ZDCs

	Absorber	Space for fibers (mm)	Modules/Layers
Prototype W-ZDC	Tungsten ($100 \times 150 \times 5$ mm^3)	1.0	$4(8\lambda_I; 218X_0)$ 27
Prototype Cu-ZDC	Copper ($100 \times 150 \times 10$ mm^3)	1.0	$8(7.5\lambda_I; 79X_0)$ 10
Production ZDC	Tungsten alloy ($100 \times 187 \times 5$ mm^3)	1.4	$3(5.1\lambda_I; 149X_0)$ 27

Table 2
Characteristics of the fiber ribbon material. NA = 0.50

	Outer diameter (mm)	Material/Index
Core	0.45	PMMA/1.49
Cladding	0.50	fluorine doped/1.40
Surface Prep	0.60	White Silicone Rubber/EMA

commercial, PMMA based[1] communication grade optical fiber. For our simulations we chose the (wavelength dependent) optical fiber attenuation coefficient and photomultiplier quantum efficiency so as to obtain agreement with the observed signal from test beam μ's. Hadronic shower simulation is based on Geisha [4] with a low energy cutoff of 0.5 MeV on electrons and photons and 1 MeV on hadrons.

The fiber sampling layers, in all cases, consist of a single ribbon of 0.5 mm diameter fibers shown in Fig. 5 as will be discussed later. We chose an orientation of 45° relative to the incident beam direction which roughly coincides with the Cherenkov angle of $\beta = 1$ particles in PMMA. PMMA fibers are readily available with a numerical aperture (NA) of 0.5 (defined as the fractional solid angle which is transmitted in the fiber). This aperture corresponds to a maximum angle of 30°. Quartz fibers generally have a smaller aperture (Tables 1 and 2).

In our simulations we studied:

(1) the effects of transverse shower leakage,
(2) energy resolution dependence on sampling frequency and photon statistics, and
(3) dependence on fiber orientation.

Fig. 2 illustrates the main advantage of the ZDC (Cherenkov) vs. scintillator sampling technique. We plot the fraction of the calorimeter signal (photons transported in the scintillator or fiber) produced as a function of radius from 100 GeV protons impacting the calorimeter. A radius of 5 cm (the maximum space allowable at the RHIC location) contains 75% of the shower signal in the case of a Pb/Scintillator calorimeter with 10 mm (Pb) and 2.5 mm (Scint) layers. The same dimension Pb calorimeter with Cherenkov sampling yields 91% containment. In general the Cherenkov technique with Pb absorber achieves a given level of containment with a factor of 2 smaller radius than with scintillator.

Changing from Pb to W absorber yields almost another factor of 2 reduction in containment radius. On the other hand, reducing the fiber numerical aperture in the sampling layer produces only a negligible change.

3.1. Cherenkov light production and capture

Since the optical fibers only transport Cherenkov light emitted nearly aligned with the fiber axis, this detector is most sensitive to charged particles which cross at approximately 45° to the fiber axis. The lower energy shower component, which is more diffuse, is therefore suppressed.

This filtering effect is reduced by multiple Coulomb scattering of electrons and by the increased path length traversed by particles with less than 45° angle to the fiber direction.

In Fig. 3 we plot the average photoelectron yields for muons and electrons traversing a ribbon

[1] Raytella fiber, Toray Industries, 600 Third Avenue, NYC 10016, USA.

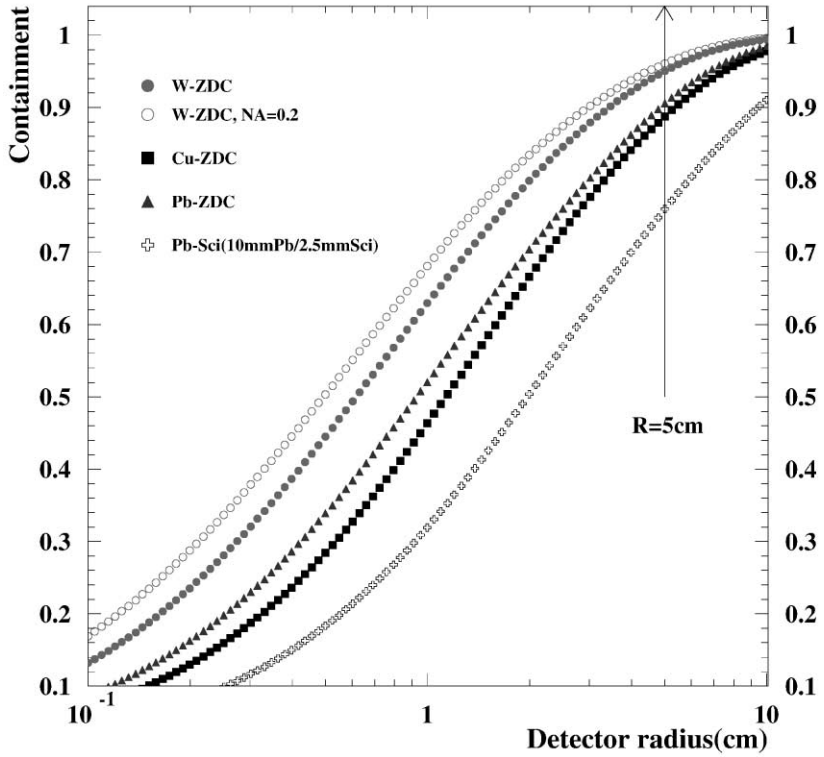

Fig. 2. Apparent shower profile for different hadron calorimeters. The W and Cu parameters are described in the text and a variant with Pb sampling is shown for comparison.

of 0.5 mm diameter fibers as a function of incidence angle. Comparing Fig. 3a and b we see that multiple Coulomb scattering has a significant effect on the response to low energy electrons. The improved angular filtering that could be obtained with lower NA fibers (see Fig. 3c) is largely offset by this effect and the lower light yield which results from small aperture.

Fig. 3d shows, in contrast, the effect (on angular dependence of yield) of removing the extra-mural absorber (black paint) from the fibers. The difference is due to "cladding modes" which are suppressed by the extra-mural absorber.

3.2. Relative response to electrons and hadrons

Fig. 4 shows the calculated response of our zdc modules to electrons and protons as a function of beam energy. In the following discussion "response" refers to signal amplitude in terms of photoelectrons produced in our PMT. The response to beam energy (100 GeV) protons is a factor of 2 lower than for electrons of the same energy. In this sense, our design is extremely non-compensating. This lack of compensation is the dominant source of energy resolution of the calorimeter for 100 GeV protons since the response changes with fluctuations in the energy fraction carried by π^o's in the hadronic shower.

3.3. Linearity

In our application, where the calorimeter is used to count beam energy neutrons, linearity is not a design consideration. It is clear from Fig. 4 that, while the response to electrons is linear with energy, the hadron response is not. Response to neutrons and protons approaches zero at low

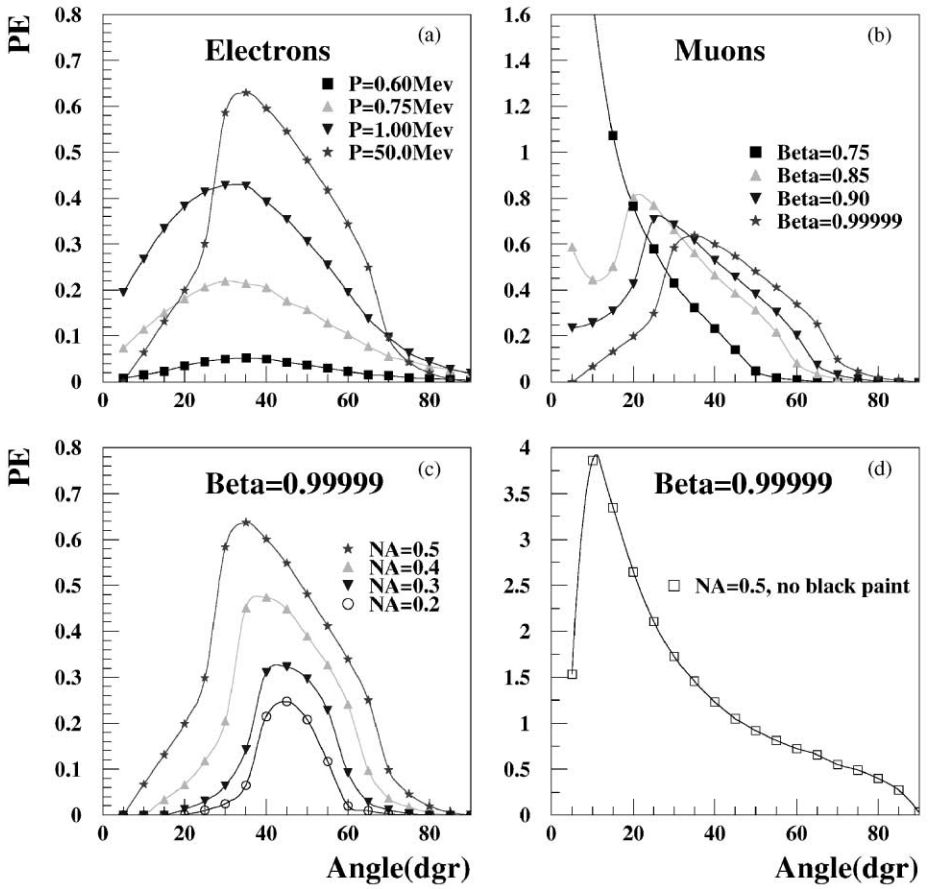

Fig. 3. Angular dependence of the photoelectron yield for 0.5 mm diameter PMMA fibers. Panel (d) illustrates the effect of removing extra-mural absorber.

energies. Also, shown in Fig. 4 is the response to muons, which has little energy dependence up to $\sim$ 100 GeV/c at which point radiative energy loss becomes significant. We use cosmic ray and beam muons for detector pre-calibration.

3.4. Energy resolution

The role of the main components of the energy resolution is illustrated in Table 3, where we fit simulated calorimeter response to 50–800 GeV proton induced showers to a stochastic plus a constant term. Our results do not fit well when these terms are added in quadrature.

If we were to increase the sampling frequency to twice our design value of 1 fiber layer per 5 mm tungsten absorber there would be a negligible change in the resolution at 100 GeV. This configuration would reduce the stochastic term due to photon statistics from 6% to 3% but leave the dominant resolution term, due to non-compensation, unchanged.

4. Module construction

For 10 cm wide modules with 5 mm absorber plates, a convenient longitudinal segmentation is one module per two nuclear interaction lengths of absorber. The total fiber area matches that of a standard 2″ PMT.

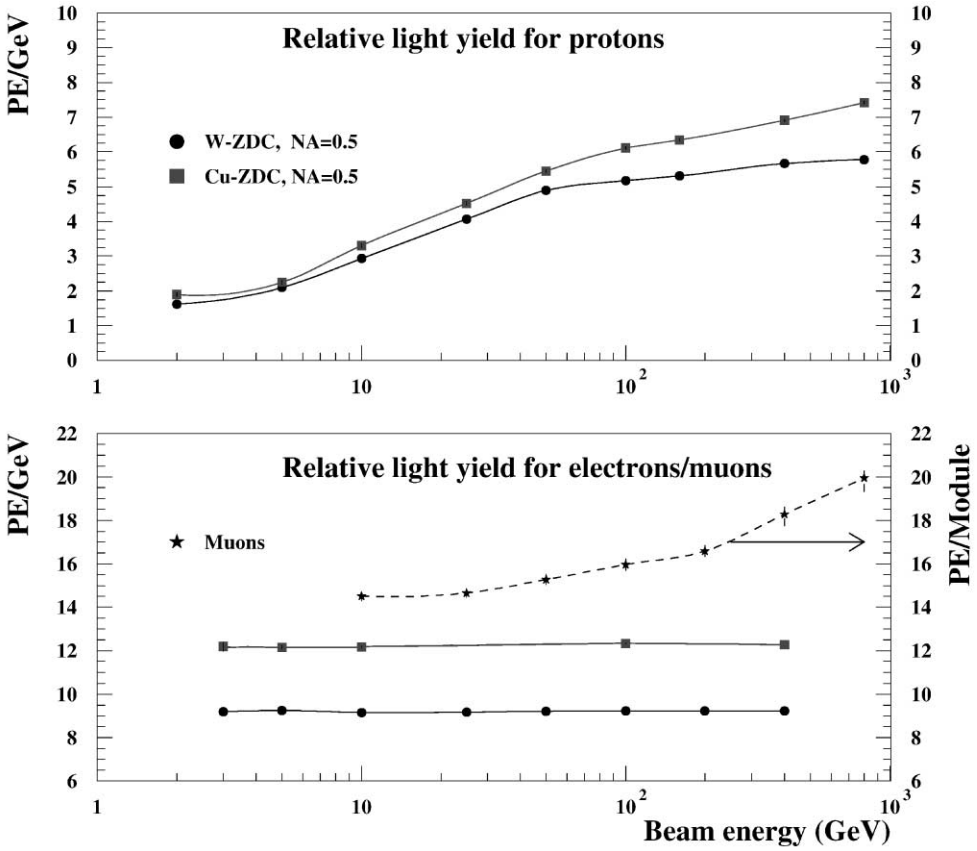

Fig. 4. Calculated response of the ZDC to protons and electrons (for both tungsten and copper modules) and muons (shown for the tungsten modules).

Table 3
Calculated energy resolution of ZDCs

Absorber	PE's per 100 Gev	"e/h" ratio	Stochastic term (%)	Constant term (%)
W (2.5 mm)	1036	1.79	69.6 ± 7.9	10.1 ± 0.7
W (5.0 mm)	518	1.78	84.6 ± 4.8	9.1 ± 0.5
W (10 mm)	256	1.78	92.4 ± 8.2	8.8 ± 0.6
Cu (10 mm)	611	2.01	111.7 ± 7.0	9.3 ± 0.6
Pb (10 mm)	422	1.80	91.0 ± 8.9	9.5 ± 0.6

For the prototype W modules we obtained 2.5 mm thick cast plates from a Russian manufacturer and bonded them in pairs. For the production modules we obtained machined plates of tungsten alloy with threaded mounting holes from a US manufacturer.[2] The thickness uniformity of our plates is ± 0.1 mm.

The fiber ribbons were wound on a mandrill and then impregnated with a low viscosity white silicone rubber glue.[3] The glue covers the active

[2] Kulite Tungsten Corporation, 160 E. Union Avenue, E. Rutherford, NJ 07073, USA.

[3] Manufactured by ETI, Fields Landing, Ca. 95537.

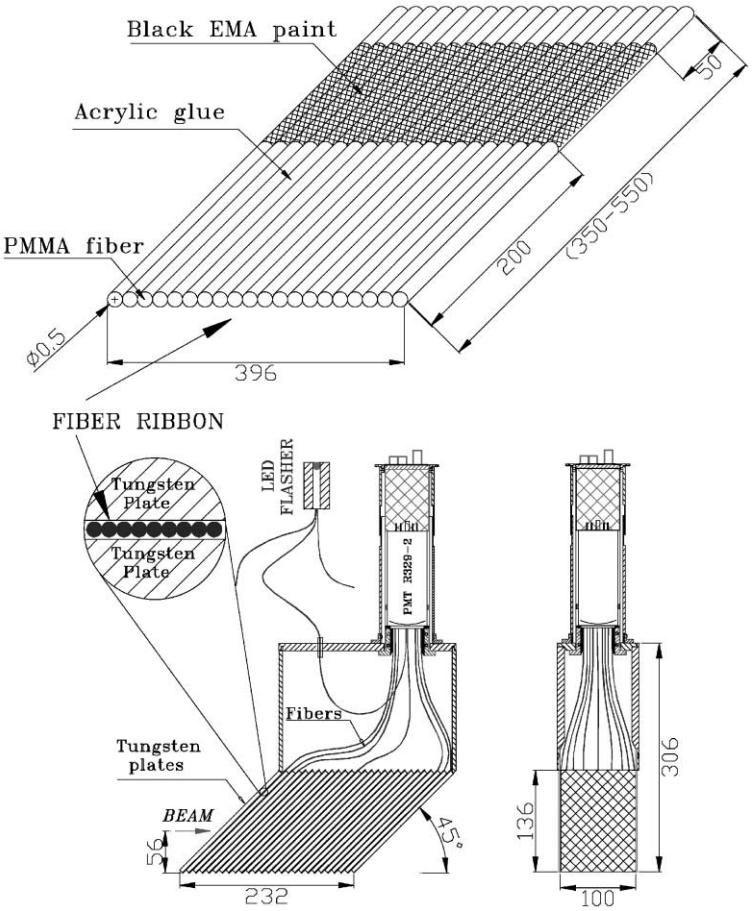

Fig. 5. Mechanical design of the production tungsten modules. Dimensions shown are in mm.

region of the fibers (200 mm) and protects the fiber surface in the region of the fiber/absorber sandwich. The light guide section of the remaining fibers is treated with an extramural absorber to suppress cladding modes in the fiber. The fiber ends closest to the PMT are collected into an acrylic compression fitting and impregnated with epoxy (Bicron BC-600). After the epoxy cured the fiber bundle was polished using a diamond tipped cutting tool on a milling machine.

The far end of the fibers were rough cut and left untreated. Our optical simulations assume no reflection at this end.

We removed three fibers at random from the ribbons in each module and coupled them to a single external optical connector for PMT gain monitoring. This allowed for stable optical connections of all modules in the calorimeter stack to a single light flasher and therefore reliable tracking of relative PMT gain.

As illustrated in Fig. 5, the fiber ribbons were trimmed to different lengths depending on their positions along the module. Lengths were adjusted to compensate for the difference in arrival time between the front and back of the module. We kept the length of the acrylic fibers to a minimum because we were concerned about the additional light production in fibers outside the absorber region, primarily due to shower leakage at the top of the calorimeter.

We selected a 12-stage general purpose PMT (Hamamatsu R329-2) [5] and mounted it with a

0.5 mm air gap from the fiber bundles. PMTs were selected for $<6\%$ photocathode non-uniformity over the 39 mm diameter area corresponding to the fiber bundle size. Linearity of the PMT and voltage divider combination is also an important criterion for this project since the calorimeters will be used to measure up to 40 or so beam energy neutrons in collisions of gold ions.

5. Pre-calibration

All modules were tested for relative light yield using cosmic muons incident along the beam axis and a standard PMT with calibrated response. Very little variation ($<10\%$) was observed among the 24 tungsten modules we eventually installed for this project.

During test beam operation we also installed trigger counters to select a small contamination of muons which were present in the proton beam. Muons traversing the full calorimeter were used to adjust relative gains of the four PMTs in the prototype calorimeter.

6. Test beam performance

The calorimeters were mounted on a table with remote x–y (transverse to the beam) positioning in the CERN North area, downstream of experiment NA49. The beam size and position were defined to ± 1 cm using a 1 cm square scintillation counter directly upstream of the table.

The main purpose of the beam test was to study the response and resolution of the calorimeter as a function of position.

The 100 and 160 GeV/c protons were selected using a beam Cherenkov counter. The beam energy spread was typically 1%. PMT current pulses were integrated and digitized using a standard commercial ADC (LRS 2249w).

7. Results

Fig. 6 shows the measured line shapes with 100 and 160 GeV incident protons. Our energy scale is normalized using the 100 GeV point. Also, shown in Fig. 6 are the expected distributions based on the Geant simulation. The distributions are well represented by a Gaussian resolution function and the response is linear over this limited energy range.

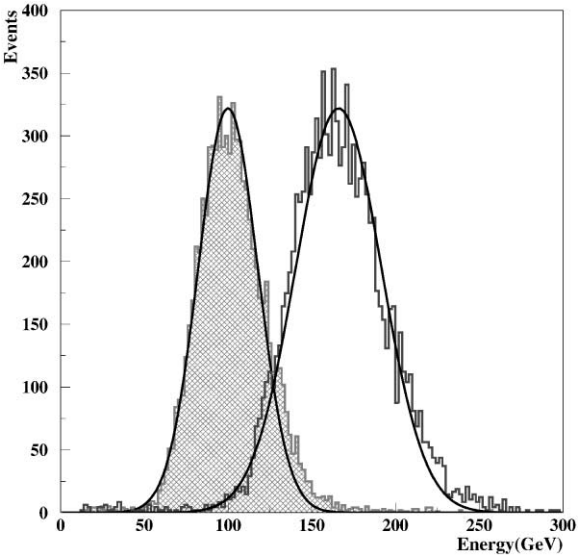

Fig. 6. Tungsten ZDC response line shapes for 100 and 160 GeV incident protons.

In Fig. 7 we plot the prototype calorimeter signal amplitude vs. impact position for both W and Cu module types. The position scans show essentially uniform response to within 1 cm of the calorimeter edge along the horizontal direction, in good agreement with simulation. In the vertical scans there is an abrupt increase in response near the upper edge of the modules. Our simulation reproduces this edge effect. It can be traced to shower leakage into the fibers above the absorber.

In order to improve module uniformity in the "beam region" we increased the height of the module in our final production design from 10 to 13.6 cm.

The tungsten calorimeter uniformity and energy resolution were essentially unchanged when the energy deposited in the fourth module was neglected. Typically 1–2% of the energy is seen in this module. The energy resolution at 100 GeV changes from 17.6% to 19% when it is removed.

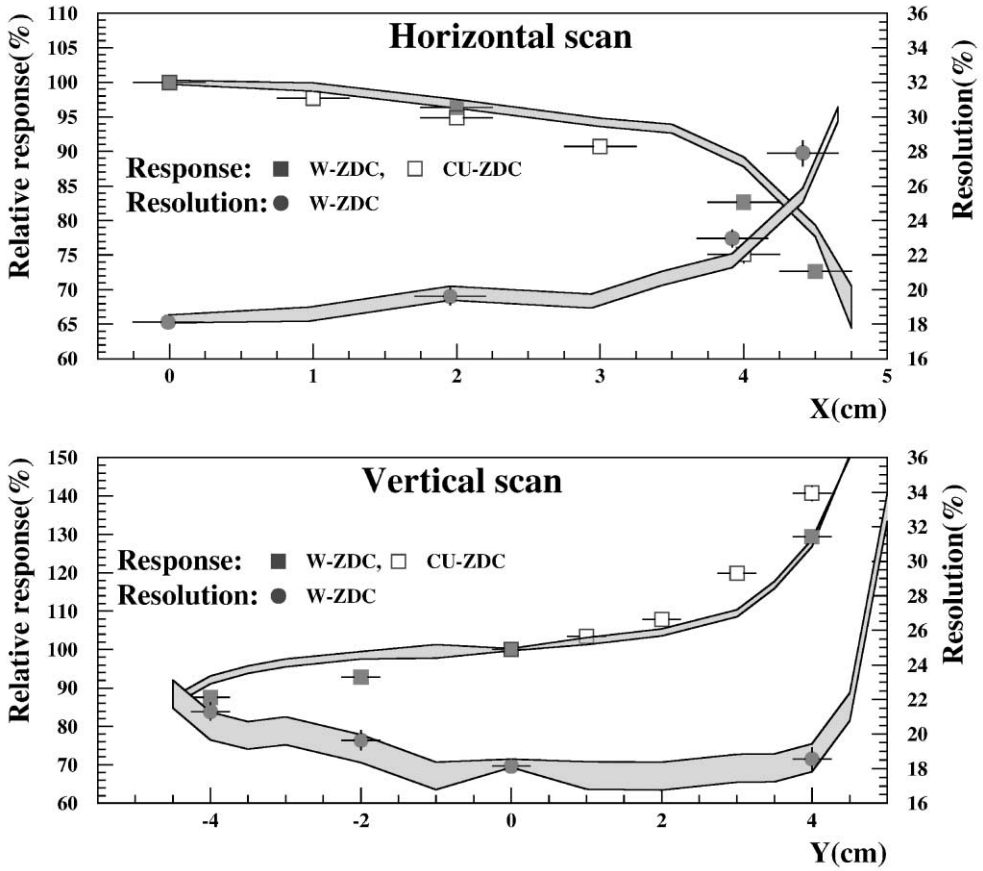

Fig. 7. Response map of the calorimeters.

In Fig. 8 we plot the resolution (r.m.s./mean) for both prototypes (using the full $8\Lambda_I$) at 100 and 160 GeV and compare them to simulation. Part of the resolution of this calorimeter is due to the unequal response to electrons and photons relative to hadrons. This introduces a limiting resolution due to fluctuations in the shower composition (i.e. π^0 vs. charged π). Hence the non-zero intercept in Fig. 8.

Our calorimeter is designed to respond to neutrons incident at the front face (45° to the fiber direction). A byproduct of the directional response of the calorimeter is that it is relatively insensitive to background particles from "beam halo" and other sources. In order to demonstrate this suppression, we inverted the calorimeter in the test beam (135° to fiber direction). The expected performance is shown in Fig. 9 together with the measured response in the two configurations. The small discrepancy in the 135° data could be accounted for by a 10% reflection coefficient at the open ends of the fiber.

7.1. Timing resolution

The ZDC signal formation is intrinsically fast. The main spread in transit time of light emitted in the fibers results from propagation along the fibers and depends on the vertical position of shower particles. A design goal of the calorimeters is to achieve better than 200 ps time-of-flight resolution. Time-of-flight measurement from the interaction to each of the ZDCs is useful since it can be used to determine the origin of beam

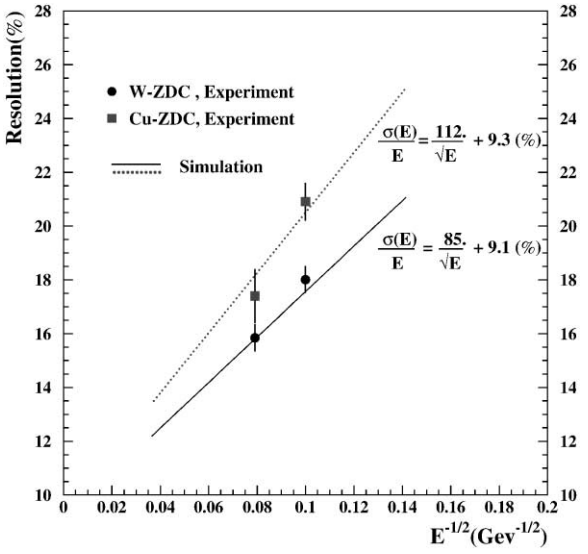

Fig. 8. The ZDC energy resolution versus energy.

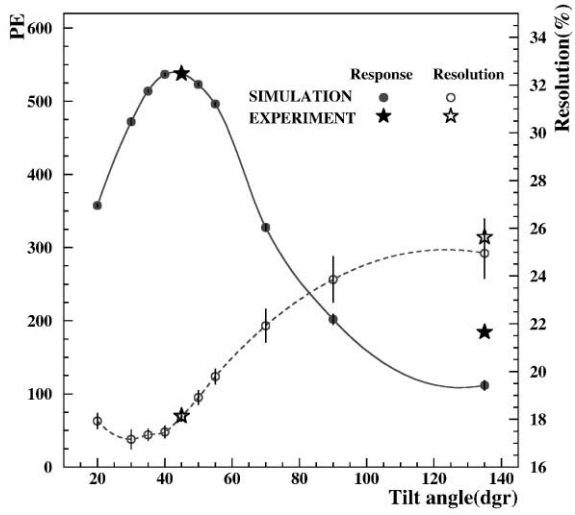

Fig. 9. The ZDC response versus angle.

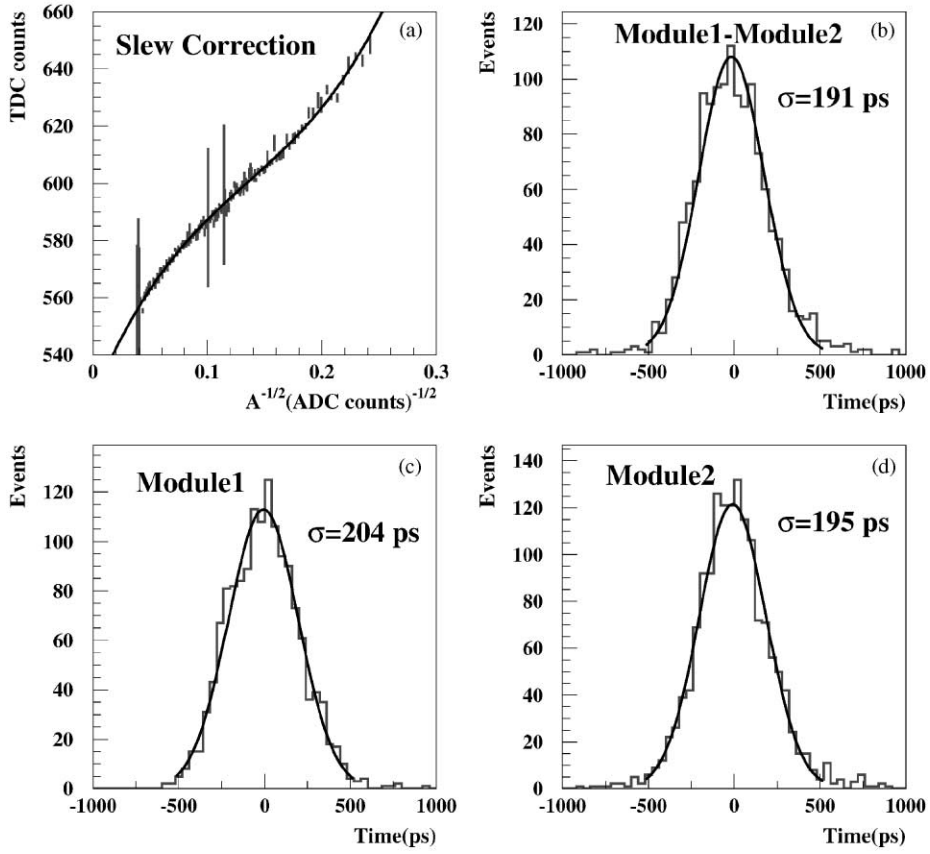

Fig. 10. Time resolution.

interactions (which is proportional to the time difference).

In practice, the arrival time of the shower will be measured by digitizing the time at which one or more PMT signals cross a threshold. We corrected the measured time taking into account the signal risetime (2.5 ns) and the measured amplitude.

Fig. 10a shows a fit to the test beam data from which we determine the slew correction. In Fig. 10b we plot the time difference between signals from modules 1 and 2. In Fig. 10c and d we plot the time difference of the two module signals compared to the beam defining scintillation counters. The resolution of the beam defining scintillators is no better than that of the ZDC but it is plausible, based on Fig. 10b, that the intrinsic ZDC resolution is $\sigma_t \leqslant 150$ ps and it is certainly better than 200 ps. With a 150 ps resolution the interaction point is measured to an error of 3 cm which is perfectly adequate for our application.

7.2. Radiation tolerance

PMMA is not a particularly radiation tolerant plastic. It is known to lose transparency more readily than polystyrene, for example. Earlier measurements on acrylic fibers [6] showed about a factor of 2 decrease in attenuation length per 10^4 Rad of gamma irradiation. Doses at the ZDC location in RHIC have been estimated at 10 kRad/yr. This is confirmed by dosimetry studies during RHIC commissioning.

We exposed one of our prototype modules to much higher integrated doses at a reactor.[4] Approximately 2/3 of the total dose was due to γ-rays and the remainder was due to neutrons. The module light output was measured using cosmic ray muons before and after three successive exposures up to a maximum of 700 kRad. The results are plotted in Fig. 11, from which we conclude that the useful lifetime of the calorimeters will be > 500 kRad.

[4] Nuclear Science Center at Texas A&M.

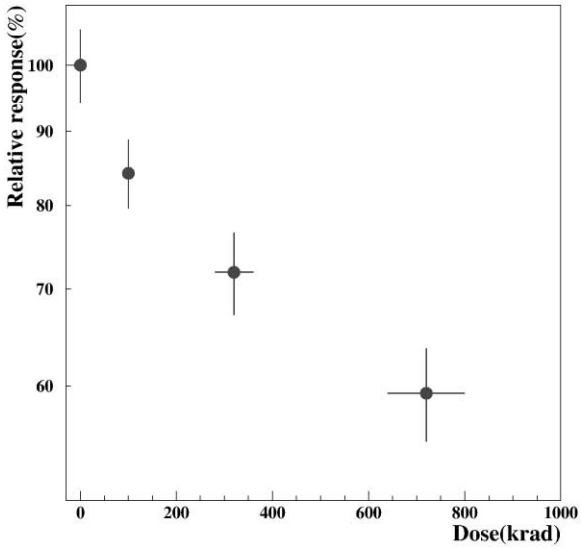

Fig. 11. Calorimeter response after radiation exposure at a reactor.

8. Production design choices

The copper and tungsten modules both had adequate performance for our application. The tungsten module yields 1–2% better energy resolution at 100 GeV and slightly better flatness of response over the calorimeter face. We chose to proceed with the tungsten module design primarily because of the $2 \times \Lambda_I$ modularity and other aspects of the mechanical design. Also the modules are more compact, which is an advantage given our limited space. The module height was increased in the production design to reduce shower leakage into the fiber bundles. Also, the calorimeter depth was reduced from 8 to $6 \times \lambda_I$ since the shorter calorimeter gives essentially identical performance.

9. Performance in RHIC

Studies of the Cherenkov/fiber sampling technique with electrons [7] have been reported elsewhere. One device [8] was built and operated in a fixed target experiment. Here we report first measurements with a 45° design hadron

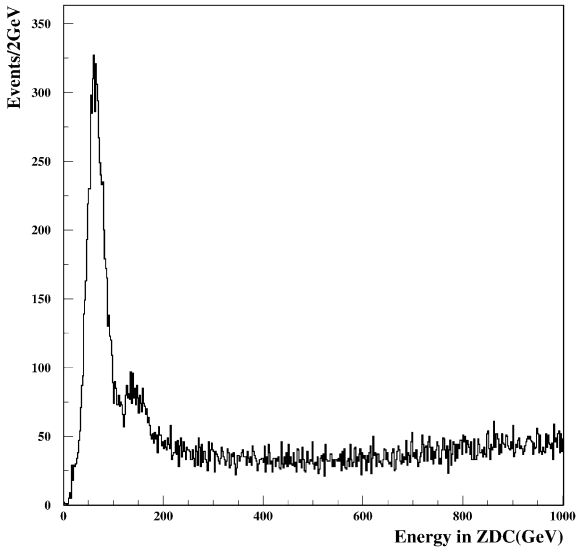

Fig. 12. Online Zero Degree Calorimeter energy distribution obtained during RHIC colliding beam operation with beam energies of 65 GeV/nucleon.

calorimeter and the first application of this method at a collider.

During the first colliding beam operation at RHIC, with gold ions accelerated to and stored at 65 GeV/nucleon beam energy, the ZDCs have been used for beam tuning and as a trigger by the RHIC experiments. Fig. 12 shows an online energy distribution from one of the calorimeters in the PHENIX experiment. The single neutron peak, which is seen clearly in this distribution, has been used to confirm the energy calibration of the calorimeters.

Acknowledgements

We wish to thank Phillipe Gorodetzky for many useful discussions throughout this project. We also thank Alice Mignerey and Bill Christie for assistance at various stages. The kind assistance of the NA49 collaboration which allowed us to share their beam line and counting house is also acknowledged. This work has been partially supported under DOE grants # DE-AC02-98CH10886, DE-FG03-93ER40773 and DE-FG02-93ER40802.

References

[1] A.J. Baltz, C. Chasman, S.N. White, Nucl. Instr. and Meth. A 417 (1998) 1, nucl-ex/9801002.
[2] H. Appelshauser et al. [NA49 Collaboration], European Phys. J. A 2 (1998) 383.
[3] A.J. Stevens, Private Communication.
[4] GEANT. Detector description and simulation tool, CERN Program Library Long Writeup W5013, CERN, Geneva, 1993.
[5] Photomultipler Tubes and Assemblies for Scintillation Counting and High Energy Physics, 1998 Catalog, Hamamatsu Photonics.
[6] J.P. de Brion, Comparative Study of Aging of PMMA and PS Optical Fibers, CEN, Saclay Report, DPHPE 86-07, 1986.
[7] M. Lundin et al., Nucl. Instr. and Meth. A 372 (1996) 359.
[8] R. Arnaldi et al., Nucl. Instr. and Meth. A 411 (1998) 1.
[9] S.N. White, Nucl. Instr. and Meth. A 409 (1998) 618.